International Journal of Theoretical and Applied Mechanics.
ISSN 0973-6085 Volume 12, Number 3 (2017) pp. 497-522

http://www.ripublication.com

Effect of Aspect Ratio on the Performance of Hydrodynamic Journal Bearing Operating Under Wear

Sanjay Sharma[1] and R K Awasthi[2]

[1]Research Scholar, I.K.Gujral Punjab Technical University, Kapurthala, Punjab-144603, India and faculty Department of Mechanical Engineering, Shri Mata Vaishno Devi University Katra-182320, India.

Email. Sanjufrnd15@gmail.com

[2]Department of Mechanical Engineering, Beant College of Engineering and Technology, Gurdaspur, Punjab-143521, India

Email. awasthi.rka@gmail.com

Abstract

The paper deals with a theoretical study concerning the effect of aspect ratio on the performance of hydrodynamic journal bearing operating under wear. The aspect ratios (L/D) are considered 0.5, 1.0 and 1.5 and for varying wear depth from 0.1 to 0.5 for the analysis of purpose. The Reynolds equations governing the flow of lubricant in the clearance space of a hydrodynamic journal bearing system with varying wear depth has been numerically solved using Galerkin's FEM. The regime is assumed to be isothermal. The positive pressure zone is established using Reynolds boundary condition through iteratively. The various performance parameters which include static, dynamic and stability terms of worn journal bearing are presented with respect to relative wear depth for varying L/D ratio and for a constant value of Sommerfeld number. The results are useful for designer for low loaded bearing only.

Keywords: FEM, aspect ratio, worn journal bearing

1. INTRODUCTION

Hydrodynamic journal bearings have been extensively used in many rotating machinery for supporting loads. While operating, these bearings normally run over a number of revolutions and are conditional to rubbing during start and stop operation.

Under these transient periods, the bearing bush progressively worn out due to abrasive method. Due to this, the geometry of bearing gets altered there by changing its performance. In the past since 1957 many investigators have examined psychological measurement of several destruct bearings [1-4]. A geometric model considers wear was first proposed by Dufrane et.al [5]. Hoshimoto et al. [6] investigated theoretically and experimentally the effect of wear on hydrodynamic journal bearing under the normal operating conditions including turbulence and observed less sensitivity for low aspect ratio. Hoshimoto et al. [7] further analyzed the effect of wear on dynamic characteristics of a rigid rotor supported by two identical symmetrically aligned bearings. Vaidyanathan and Keith [8] analyzed four bearing: circular, worn, two-lobe and elliptical considering the effects of turbulence and cavitation. Suzuki and Tanaka [9] in 1995 examined the stability characteristics of a hydrodynamic worn journal bearing. Kumar and Mishra [10, 11] found that due to wear the friction, flow rate increases and the load capacity, stability are reduces. Fillon and Bouyer [12] have conducted thermohyrodynamic study of a worn journal bearing under transient conditions and examined the effect of wear on bearing performance characteristics for varying speed and load. Some literature is also available for the worn hybrid and hydrostatic journal bearing used in high-pressure fluid applications [13-17].

A study of bearing dynamics is important for enhancing smooth bearing life. An understanding on how bearing size (aspect ratio) influences bearing performance of hydrodynamic journal bearing with different stages of wear due to start/stop motion is yet to be revealed. As there appears to be a very little work obtain in the published literature taking into consideration the effect of aspect ratio on journal bearing system with different magnitude of wear depth. Thus the motivation behind theoretical study is a depth understanding about the role of aspect ratio on static, dynamic and stability aspect of hydrodynamic journal bearing owing to wear.

In order to account the wear, a numerical model for wear depth used by Dufrane et al. [5] has been considered in the analysis. The governing equation for hydrodynamic lubrication is solved using FEM. The details have been given in section 2.

2. ANALYSIS

The conventional Reynolds equation for an incompressible, Newtonian lubricant in the clearance space of a finite journal bearing system is given below in non-dimensional form as [13-14]:

$$\frac{\partial}{\partial\alpha}\left(\frac{\bar{h}^3}{12}\frac{\partial\bar{p}}{\partial\alpha}\right)+\frac{\partial}{\partial\beta}\left(\frac{\bar{h}^3}{12}\frac{\partial\bar{p}}{\partial\beta}\right)=\frac{\Omega}{2}\frac{\partial\bar{h}}{\partial\alpha}+\frac{\partial\bar{h}}{\partial\tau} \tag{1}$$

The conventional Reynolds Eq. (1) is solved using FEM, which is described below.

2.1 Fluid-Film Thickness

The worn bearing zone geometry is shown in Fig.1. A non-dimensional parameter $\bar{\delta}_w$ has been taken and consider as the measure of wear. Based on the visual examination, Dufrane et al. [5] presume an abrasive wear model they consider that due to frequently start and start operation of bearing. The footmark left by the shaft is uniform at the base of the bearing and the wear design is uniform along its axial length. Due to this, the bush geometry changes and shown as: [5, 12]

$$\partial\bar{h} = \bar{\delta}_w - 1 - \sin\alpha \text{ ; for } \alpha_b \le \alpha \le \alpha_e \tag{2}$$

$$\partial\bar{h} = 0 \text{ ; for } \quad \alpha < \alpha_b \text{ or } \alpha > \alpha_e \tag{3}$$

The angles α_b and α_e are at the beginning and end of the footmark, respectively. The angles α_b and α_e are calculated from Eq. (2) and (3), as $\sin\alpha = \bar{\delta}_w - 1$. Taking the values of computed journal center coordinates ($\bar{X}_J$ and $\bar{Z}_J$) and defect value $\partial\bar{h}$ is added to the calculated fluid-film thickness, expressed as [10-12]

$$\bar{h} = 1 - \bar{X}_J \cos\alpha - \bar{Z}_J \sin\alpha + \partial h \tag{4}$$

The eccentricity ratio is given by

$$\varepsilon = \sqrt{\left|\bar{X}_J\right|^2 + \left|\bar{Z}_J\right|^2} \tag{5}$$

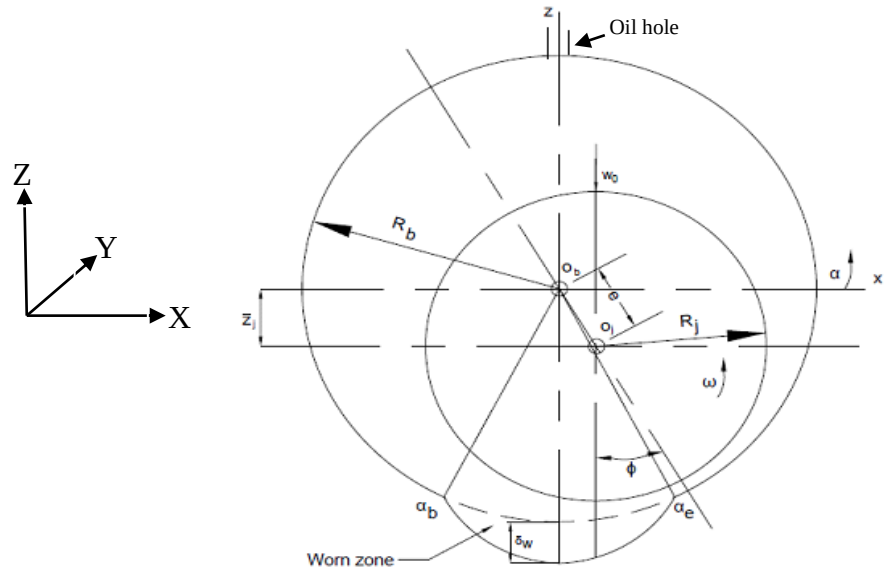

Figure 1: Worn bearing geometry

2.2 FEM Formulation

The lubricant domain is discretised using four noded quadrilateral isoparametric elements. The weighted residual of Eq. (1) using Galerkin's criteria may be expressed as [17, 23]:

$$\iint_{A^e}\left\{\frac{\partial}{\partial\alpha}\left(\frac{\bar{h}^3}{12}\frac{\partial\bar{p}^e}{\partial\alpha}\right)+\frac{\partial}{\partial\beta}\left(\frac{\bar{h}^3}{12}\frac{\partial\bar{p}^e}{\partial\alpha}\right)-\frac{\Omega}{2}\frac{\partial\bar{h}}{\partial\alpha}-\frac{\partial\bar{h}}{\partial\tau}\right\}N_i\,d\alpha d\beta=0 \tag{6}$$

where N_i is the interpolation function relating the nodal pressures $\bar{p}_j$ to the pressure in the e[th] element of the discretized pressure field of N finite elements,[23] i.e.,

$$\bar{p}^e=\sum_{j=1}^{n^e}N_j\bar{p}_j \tag{7}$$

where N_j is the elemental shape function and n^e is number of nodes per element.

With simplifications, Eqs. (6) and (7) give the element Eq. as[13]:

$$\left[\bar{F}^e\right]_{n^e\times n^e}\left\{\bar{p}^e\right\}_{n^e\times 1}=\left\{\bar{Q}^e\right\}_{n^e\times 1}+\Omega\left\{\bar{R}_H{}^e\right\}_{n^e\times 1}+\dot{\bar{x}}\left\{\bar{R}_{X_J}{}^e\right\}_{n^e\times 1}+\dot{\bar{z}}\left\{\bar{R}_{Z_J}{}^e\right\}_{n^e\times 1} \tag{8}$$

where $\dot{x}$ and $\dot{z}$ are the journal centre velocity.

For an e^{th} element, each elements of Eq.(8) is described as:

$$\bar{F}_{ij}{}^e=\iint_{A^e}\bar{h}^3\left[\frac{1}{12}\frac{\partial N_i}{\partial\alpha}\frac{\partial N_j}{\partial\alpha}+\frac{1}{12}\frac{\partial N_i}{\partial\beta}\frac{\partial N_j}{\partial\beta}\right]d\alpha\,d\beta \tag{9}$$

$$\bar{Q}_i^e=\int_{\Gamma^e}\left\{\left(\frac{\bar{h}^3}{12}\frac{\partial\bar{p}^e}{\partial\alpha}-\frac{\Omega\bar{h}}{2}\right)l+\left(\frac{\bar{h}^3}{12}\frac{\partial\bar{p}}{\partial\beta}\right)m\right\}N_i\,d\bar{\Gamma}^e \tag{10}$$

$$\bar{R}_{H_i}^e=\iint_{A^e}\frac{\bar{h}}{2}\frac{\partial N_i}{\partial\alpha}\,d\alpha\,d\beta \tag{11}$$

$$\bar{R}_{X_{J_i}}{}^e=\iint_{A^e}N_i\cos\alpha\,d\alpha\,d\beta \tag{12}$$

$$\bar{R}_{Z_{J_i}}{}^e=\iint_{A^e}N_i\sin\alpha\,d\alpha\,d\beta \tag{13}$$

where l and m are the directions cosines and i, j =1,2 … n^e .

The assembly of Eq. (8) over the entire domain of pressure field results global linear equations and expressed as:

$$\left[\overline{F}\right]_{N\times N}\left\{\overline{p}\right\}_{N\times 1}=\left\{\overline{Q}\right\}_{N\times 1}+\Omega\left\{\overline{R}_{H}\right\}_{N\times 1}+\dot{\overline{x}}\left\{\overline{R}_{X_J}\right\}_{N\times 1}+\dot{\overline{z}}\left\{\overline{R}_{Z_J}\right\}_{N\times 1} \tag{14}$$

Where N, number of nodes in the entire domain, involving the pressure $\{\overline{p}\}$ and the flow $\{\overline{Q}\}$as nodal variables.

2.3 Boundary conditions

The boundary conditions used for the solution are described as:

$$\left.\begin{array}{l} Nodes\ on\ external\ boundary,\ \overline{P}=\pm 1.0\ \ at\ \ \beta=\pm 0.5,1,1.5 \\ At\ the\ trailing\ edge\ of\ \ positive\ region,\ \ \overline{p}=\dfrac{\partial \overline{p}}{\partial \alpha}=0.0 \\ pressure\ at\ leading\ edge\ and\ centre\ hole\ is\ considered\ to\ be\ atmosphere \\ and\ therefore\ \overline{p}=0.0 \end{array}\right\} \tag{16}$$

Eq. (9) can be solved to give both pressure and flow simultaneously because at each node one of the two variables is known.

The static performance characteristics are computed for the steady-state condition, i.e., $\dot{\overline{x}}=\dot{\overline{z}}=0$. It is essential to establish the journal center equilibrium position for the evaluation of performance characteristics at a given vertical load.

2.4 Journal Center Equilibrium Position

For a given vertical external load $\overline{W_o}$ or eccentricity ratio ε and operating and geometric parameters of the bearing, the journal center position ($\overline{X}_J, \overline{Z}_J$) is unique. This journal center equilibrium position is not known a priori and is obtained iteratively. For a specified vertical external load ($\overline{W_o}$), which acts parallel to the Z-axis and when the journal center occupies its equilibrium position, the fluid-film reaction components must satisfy the following conditions.

$$\left.\begin{array}{l} \overline{F}_x=0 \\ \overline{F}_z-\overline{W_o}=0 \end{array}\right\} \tag{17}$$

Initially the tentative values of journal center coordinates ($\overline{X}_J, \overline{Z}_J$) are fed as input to compute the nominal fluid-film thickness ($\overline{h}$) that is required for the computation of

fluid-film pressures. The fluid-film reaction components $\overline{F}_x$ and $\overline{F}_z$ are computed using Eqs. (18) and (19), respectively.

2.5 Load Carrying Capacity ($\overline{F}$)

Fluid-film reaction components along X and Z directions are respectively given by [18, 19]

$$\overline{F}_x = -\int_{-\lambda}^{\lambda}\int_{0}^{2\pi} \overline{p}\cos\alpha \, d\alpha \, d\beta \tag{18}$$

and

$$\overline{F}_z = -\int_{-\lambda}^{\lambda}\int_{0}^{2\pi} \overline{p}\sin\alpha \, d\alpha \, d\beta \tag{19}$$

Then, the resultant fluid-film reaction is expressed as

$$\overline{F} = \left[\overline{F}_x^{\,2} + \overline{F}_z^{\,2}\right]^{1/2} \tag{20}$$

2.6 Sommerfeld Number

The bearing characteristic number, is a dimensionless quantity used extensively in hydrodynamic lubrication analysis and is usually expressed as a function of a single parameter called the Sommerfeld Number [22].The Sommerfeld number can be determined as:

$$S = \frac{2\left(\frac{L}{D}\right) p_s R_j^{\,2}}{\pi W_0} \tag{21}$$

2.7 Attitude Angle (ϕ)

The angle between the line joining bearing, journal center and load line is defined as attitude angle. The attitude angle ϕ is calculated by:

$$\phi = \tan^{-1}\left[\frac{\overline{\overline{X}}_J}{\overline{\overline{Z}}_J}\right] \tag{22}$$

2.8 Friction Force

The friction force in a journal bearing is computed from the following equation [10-11]:

$$\bar{F}_L = \sum_{e=1}^{n_e} \int_{A^e} \left(\Omega \frac{\bar{\tau}_c}{\bar{h}} + \frac{\bar{h}}{2} \frac{\partial \bar{p}}{\partial \alpha} \right) dA \tag{23}$$

where $\bar{\tau}_c$ is the normalized couette shearing stress. For laminar flow, $\tau = 1.0$ and Coefficient of friction, $f\left(\frac{R_j}{c}\right) = \frac{\bar{F}_l}{\bar{F}}$.

2.9 Fluid-Film Stiffness and Damping Coefficients

A journal bearing system has two degrees of freedom to define the journal position during its oscillation. Considering two degrees of freedom system, 2x2 fluid-film stiffness and 2x2 fluid-film damping coefficients can be computed using the expressions given below. The fluid-film stiffness coefficients are expressed as [26, 27]:

$$\bar{S}_{ij} = -\frac{\partial \bar{F}_i}{\partial \bar{q}_J}, \ (i = x, z) \tag{24}$$

Where,

i = direction of force.

$\bar{q}_J$ = direction of journal center displacement ($\bar{q}_J = \bar{x}, \bar{z}$).

Stiffness coefficient matrix will be

$$\begin{bmatrix} \bar{S}_{xx} & \bar{S}_{xz} \\ \bar{S}_{zx} & \bar{S}_{zz} \end{bmatrix} = -\begin{bmatrix} \frac{\partial \bar{F}_x}{\partial \bar{x}} & \frac{\partial \bar{F}_x}{\partial \bar{z}} \\ \frac{\partial \bar{F}_z}{\partial \bar{x}} & \frac{\partial \bar{F}_z}{\partial \bar{z}} \end{bmatrix} \tag{25}$$

The fluid-film damping coefficients are expressed as [26, 27]:

$$\bar{C}_{ij} = -\frac{\partial \bar{F}_i}{\partial \dot{\bar{q}}_J}, \ (i = x, z) \tag{26}$$

$\dot{q}$ represents the velocity component of journal center ($\dot{\bar{x}}, \dot{\bar{z}}$).

Damping coefficients matrix is given by:

$$\begin{bmatrix} \overline{C}_{xx} & \overline{C}_{xz} \\ \overline{C}_{zx} & \overline{C}_{zz} \end{bmatrix} = -\begin{bmatrix} \dfrac{\partial \overline{F}_x}{\partial \dot{\overline{x}}} & \dfrac{\partial \overline{F}_x}{\partial \dot{\overline{z}}} \\ \dfrac{\partial \overline{F}_z}{\partial \dot{\overline{x}}} & \dfrac{\partial \overline{F}_z}{\partial \dot{\overline{z}}} \end{bmatrix} \tag{27}$$

2.10 Critical mass

The non-dimensional critical mass $\overline{M}_c$ of the journal is expressed as [17]:

$$\overline{M}_c = \frac{\overline{G}_1}{\overline{G}_2 - \overline{G}_3} \tag{28}$$

Where,

$$\overline{G}_1 = \left[\overline{C}_{xx}\overline{C}_{zz} - \overline{C}_{zx}\overline{C}_{xz}\right],\ \overline{G}_2 = \frac{\left[\overline{S}_{xx}\overline{S}_{zz} - \overline{S}_{zx}\overline{S}_{xz}\right]\left[\overline{C}_{xx} + \overline{C}_{zz}\right]}{\left[\overline{S}_{xx}\overline{C}_{zz} + \overline{S}_{zz}\overline{C}_{xx} - \overline{S}_{xz}\overline{C}_{zx} - \overline{S}_{zx}\overline{C}_{xz}\right]} \quad \text{and}$$

$$\overline{G}_3 = \frac{\left[\overline{S}_{xx}\overline{C}_{xx} + \overline{S}_{xz}\overline{C}_{xz} + \overline{S}_{zx}\overline{C}_{zx} + \overline{S}_{zz}\overline{C}_{zz}\right]}{\left[\overline{C}_{xx} + \overline{C}_{zz}\right]}$$

2.11 Threshold speed

The threshold speed of instability, is expressed as [14]:

$$\overline{\omega}_{th} = \left[\overline{M}_c \big/ \overline{F}_o\right]^{1/2} \tag{29}$$

Where , $\overline{F}_0$ is the resultant fluid-film force or reaction $\left(\dfrac{\partial \overline{h}}{\partial \overline{t}} = 0\right)$. A journal bearing system is asymptotically stable when the journal mass $\overline{M}_J$ is less than the critical mass $\overline{M}_c$ (i.e. when $\overline{M}_J < \overline{M}_c$). Simillarly, when the operating speed of the journal is less than the threshold speed (i.e. when $\Omega < \overline{\omega}_{th}$) then the system is asymptotically stable. The solution process is expressed in flow chart shown in Fig.2.

2.12 Whirl frequency ratio

Whirl frequency ratio $\overline{\omega}_{whirl}$ can expressed in simplified form as [17, 21]:

$$\overline{\omega}_{whirl}{}^{2} = \frac{K_1}{\overline{M}_c} \tag{30}$$

where K_1 is expressed as:

$$K_1 = \frac{\overline{S}_{xx}\overline{C}_{zz} + \overline{S}_{zz}\overline{C}_{xx} - \overline{S}_{xz}\overline{C}_{zx} - \overline{S}_{zx}\overline{C}_{xz}}{\overline{C}_{xx} + \overline{C}_{zz}}$$

The lower the value of $\overline{\omega}_{whirl}$, the higher will be stability. The negative value of $\overline{\omega}^{2}{}_{whirl}$ implies the absence of the whirl.

3. SOLUTION PROCEDURE

The accuracy of a numerical result generally depends on the size of the computational grid. A good strategy is to simulate and compute results using small number of grid points and then keep on increasing the number of grid points until the numerical results doesn't change perceptibly. This procedure is adopted to ascertain that the inaccuracies in the numerical results are atleast not due to the grid size. For the present study, the similar procedure has been adopted to select the optimal grid size. The computer code designed for the current study is quite user friendly. The code automatically describes the domain for specified elements in circumferential and axial direction at a specified eccentricity ratio. First, elements in x-direction (circumferential direction) are varied and elements in y-direction (axial direction) are kept fixed. The eccentricity ratio has been specified to be 0.5. The variation of elements in circumferential direction is limited to 146 and in axial direction it is fixed (4) initially. The optimal grid has been selected on the basis of consistency in the value of load carrying capacity. It may be seen in Fig. 2(a), that the non-dimensional value of load carrying capacity ($\overline{W}$) vary significantly up to thirty six number of elements. However after increasing circumferential elements beyond thirty six, the variation in the ($\overline{W}$) becomes very low. It may be observed from Fig. 2(b) that for a higher elements in circumferential direction the processing time increase enormously for a slight improvement in the value of $\overline{W}$.From the observation of Figures 2(a) and 2(b), for a chosen number of elements in circumferential direction is to be 36, the computation time is not much large, for satisfaction in value of$\overline{W}$.

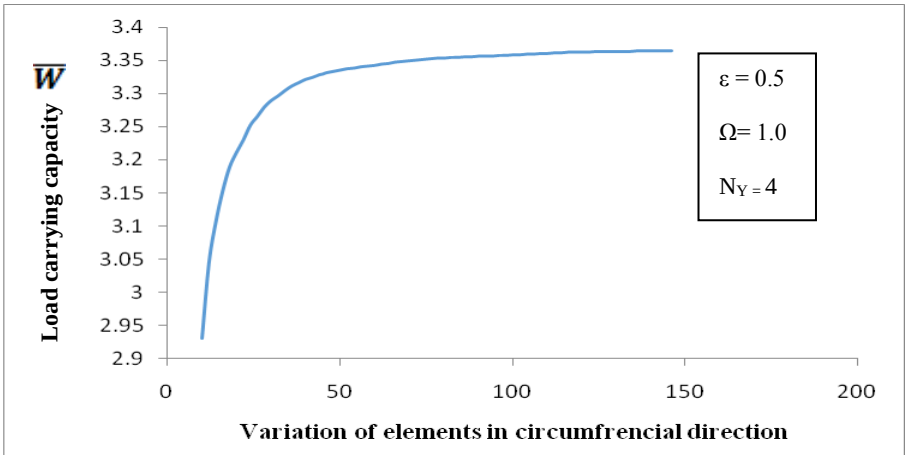

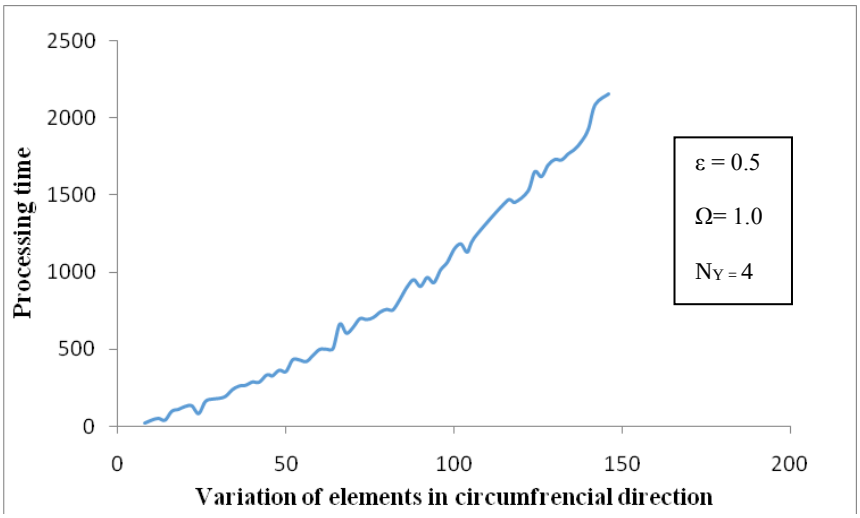

Figure 2(a) Load carrying capacity versus variation of elements in circumferential direction. Fig. 2(b) Processing time versus variation of elements along circumferential direction

The study of transient wear through numerical simulation has been performed using flow chart as shown in Fig. 3. The simulation is performed using following steps.

1. The fluid-film domain is automatically discretised into four noded quadrilateral isoparametric elements by assigning number of elements in circumferential and axial direction.
2. Fluid-film pressure field are initialized by assigning an arbitrary value of journal centre.
3. Fluid-film thickness is calculated using Eq. (4).

4. A two point Gauss quadrature is used for the integration in elements. Thus four Gauss points are generated in an quadrilateral isoparametric element.
5. Element equations are assembled using indexing to obtain global system of matrices and then boundary conditions are implemented. Cavitation boundary is established using iteration.
6. Newton's iterative method is used for establishing journal centre equilibrium.
7. Steps 2-6 are repeated until the equilibriums established.

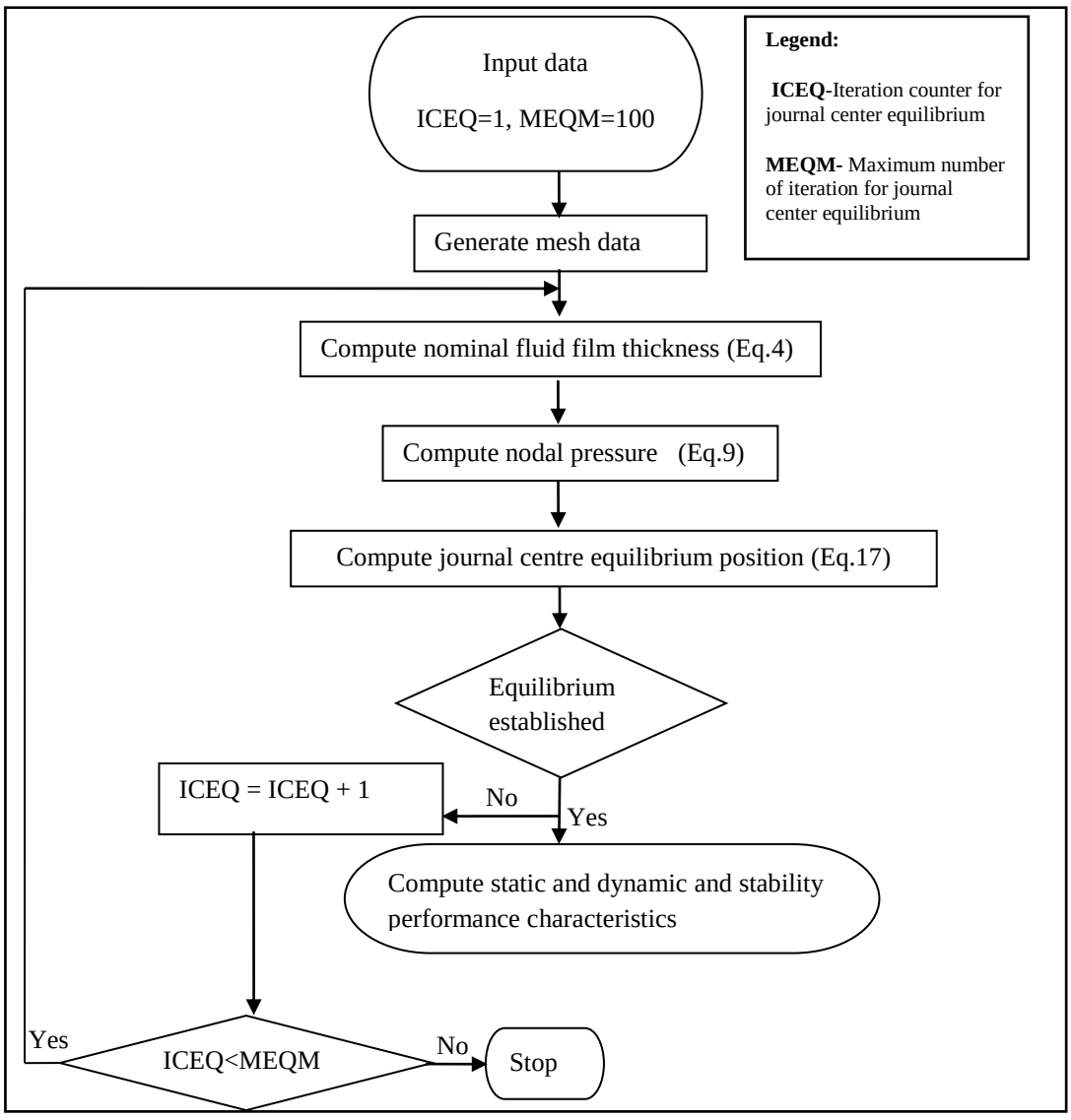

Figure 3: Overall solution process scheme

The simulated data for non dimensional bearing performance parameters have been generated and plotted to gain understanding. The results have been discussed in the following paragraphs.

3.1 Results and Discussion

The performance characteristics for a worn journal bearing system with various wear depth have been presented and discussed in this section. The influence of wear depth on the performance characteristics of worn journal bearing system have been computed by developed computer code in Fortran 90.

In order to validate the developed program, the numerically simulated results for eccentricity ratio (ε) corresponding to different values of the Sommerfeld number for wear depth $\bar{\delta}_w = 0.0$ and 0.2 are computed from the present study and compared with the already published results in literature [6, 7] as shown in Figure.4.The results are observed to be in good agreement with the published work and thus establishes the accuracy of developed code. The bearing geometric and operating parameter values are selected based on the published literature and are shown in Table 1.

Table 1: Operating and Geometric Parameters of Worn Hydrodynamic Journal Bearing.

Table 1: OPERATING AND GEOMETRIC PARAMETERS	
PARAMETERS	**VALUE/ RANGE**
Sommerfeld Number (S)	0.8
Speed parameter (Ω)	1.0
Wear depth parameter ($\bar{\delta}_w$)	0.0 - 0.5
Aspect ratio $\left(\frac{L}{D}\right)$	0.5, 1.0 and 1.5
Clearance ratio $\left(\frac{c}{R}\right)$	0.001

The simulated results of worn journal bearing with respect to relative wear depth for varying L/D ratio and for a constant value of Sommerfeld number is presented. Thus the results are useful for low loaded bearing only. The percentage changes in static and dynamic performance of hydrodynamic journal bearing operating under transient wear are reported in Table 2 and Table 3 respectively.

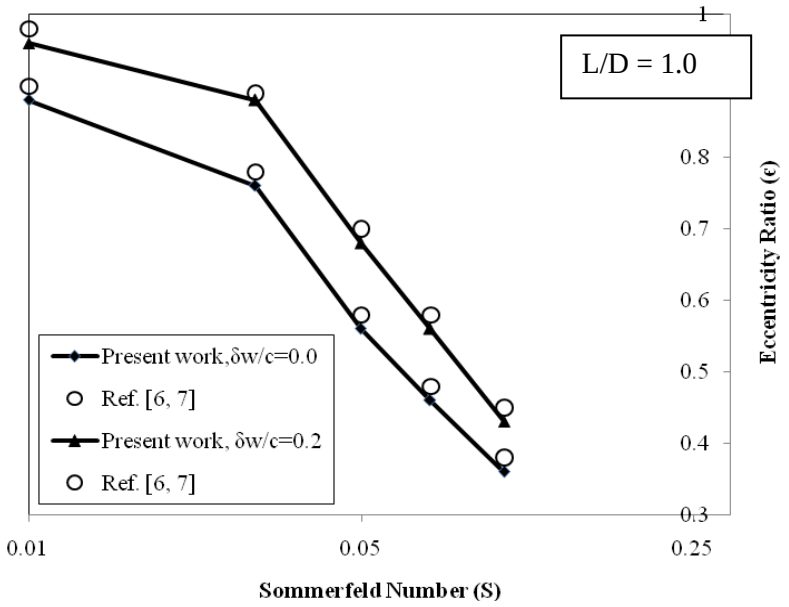

Figure 4: Eccentricity ratio versus Sommerfeld number (hydrodynamic journal bearing)

Figure.5 shows that the bearing with L/D ratio of 0.5 has higher eccentricity ratio than other L/D ratios. It is observed that the increase in L/D ratio decreases the eccentricity ratio. It is also observed that eccentricity ratio increases more rapidly after $\overline{\delta}_w > 0.3$. The percentage change in the value of eccentricity ratio due to wear between L/D ratio of 0.5,1.0 and 1.5 found to be more after $\overline{\delta}_w > 0.3$ as presented in Table 2. This is because journal tends to go inside the cavity formed due to wear. The greater the wear depth, greater the eccentricity of the bearing.

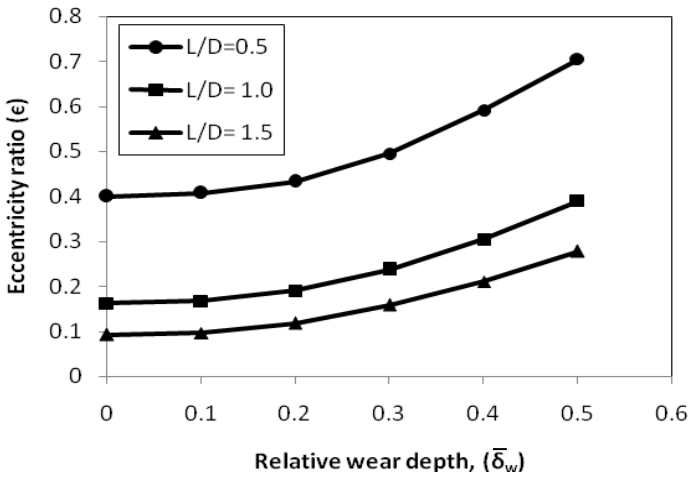

Figure 5: Eccentricity ratio versus relative wear depth

Figure.6 shows that the effect of wear on the value of maximum pressure is significantly higher for bearing with L/D ratio of 0.5 as compared to other L/D ratios. It is also observed that the value of maximum pressure for a specified relative wear depth decreases with an increase in L/D ratio. It is also observed that the percentage change in the value of maximum pressure due to wear between L/D ratio of 0.5,1.0 and 1.5 found to be more when $\bar{\delta}_w < 0.3$ as presented in Table 2.

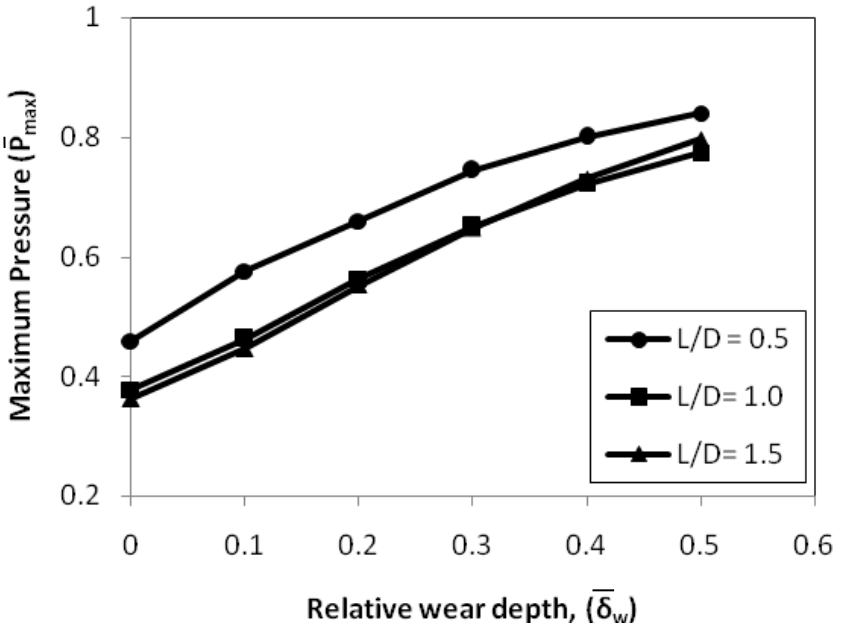

Figure 6: Maximum pressure versus relative wear depth

In Fig.7 it is observed that the value of minimum fluid-film thickness for a specified relative wear depth increases with the increase in L/D ratio and decrease with an increase in wear depth.The reduction in the value of fluid-film thickness is quite significant at lower L/D ratio of 0.5. It is also observed that the value of minimum fluid-film thickness decreases more rapidly when $\bar{\delta}_w > 0.2$. The percentage change in the value of minimum fluid-film thickness due to wear between L/D ratio of 0.5, 1.0 and 1.5 found to more at lower L/D ratio of 0.5 and decrease with an increase in L/D ratio as reported in Table 2.

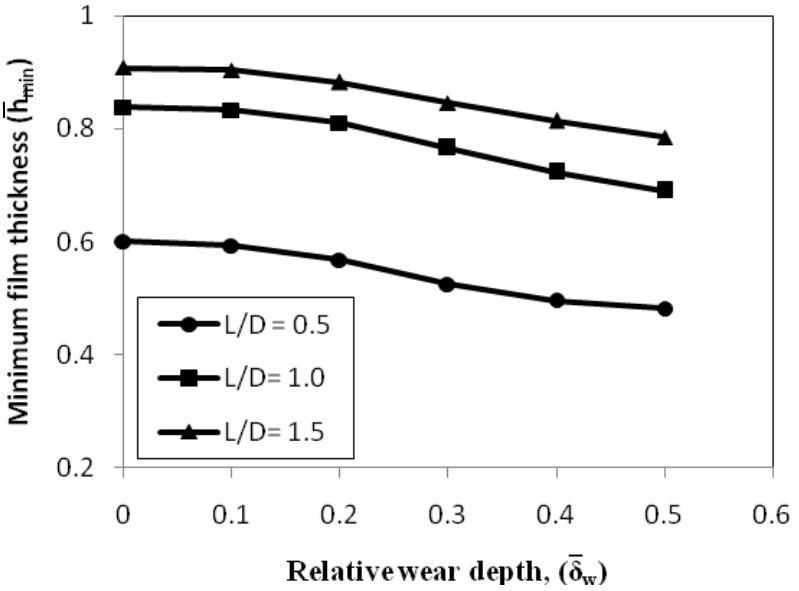

Figure 7: Minimum fluid-film thickness versus relative wear depth

In Fig.8 attitude angle decreases with increases in relative wear depth and L/D ratio. The percentage change in the value of attitude angle due to wear between L/D ratio of 0.5, 1.0 and 1.5 found to be more at higher L/D ratio of 1.5 as reported in Table 2. The percentage variation in the value of attitude angle between lower L/D ratio of 0.5 and 1.0 are approximate same after $\bar{\delta}_w > 0.3$ as reported in Table 2.

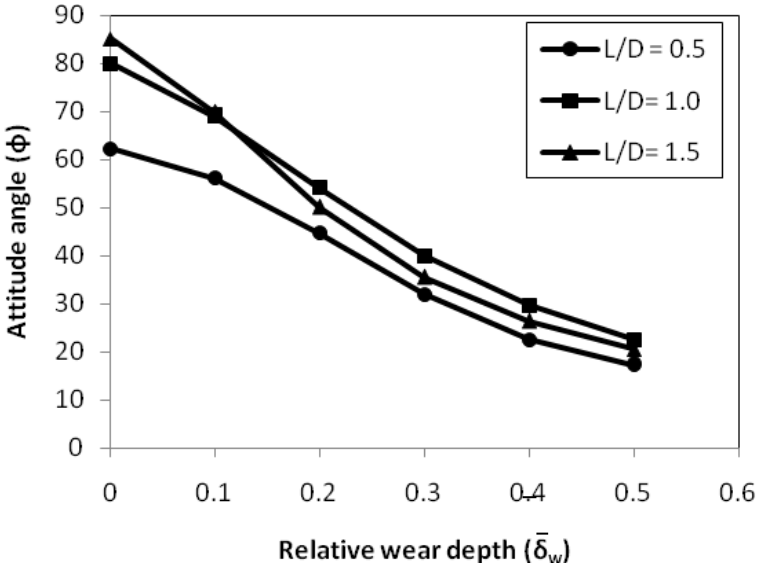

Figure 8: Attitude angle versus relative wear depth

In Fig.9 friction coefficient is increased with increasing in wear depth and decrease with increased in L/D ratio. It is also observed that the value of coefficient of friction increases more rapidly when $\bar{\delta}_w > 0.2$ at lower L/D ratio of 0.5.The percentage change in the value of friction coefficient due to wear between L/D ratio of 0.5, 1.0 and 1.5found to be more at lower L/D ratio of 0.5 as reported in Table 2. The results shows, that there is judicious need to select optimal L/D ratio from the view point of frictional power loss and load carrying capacity of fluid film journal bearing.

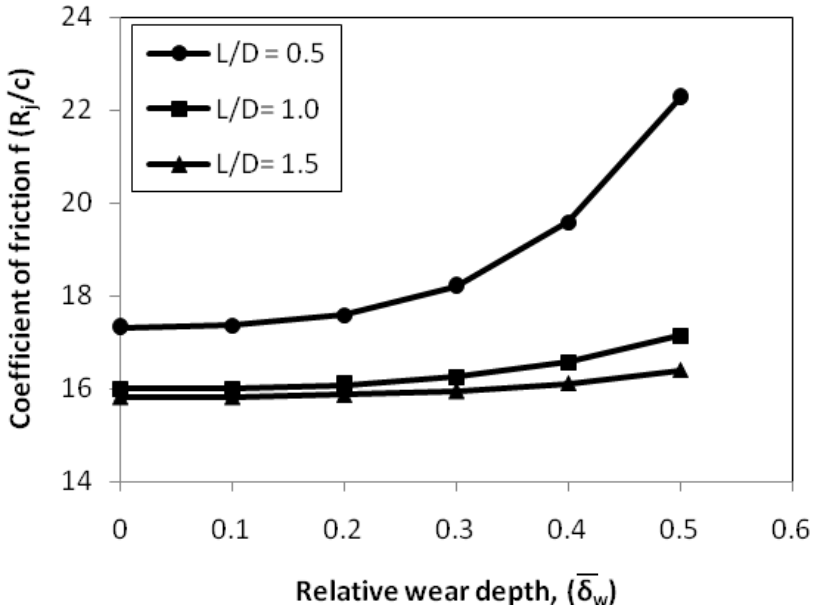

Figure 9: Coefficient of friction versus relative wear depth

The direct fluid-film stiffness coefficients $\bar{S}_{xx}$ and $\bar{S}_{zz}$ as shown in fig.10 and fig.11 shows a increasing trend with an increase in L/D ratio and wear depth. It is also observed that direct fluid-film stiffness coefficient $\bar{S}_{xx}$ parameters increases more rapidly when $\bar{\delta}_w > 0.2$ at lower L/D ratio of 0.5 but on the other hand in case of direct fluid-film stiffness coefficients $\bar{S}_{zz}$ parameters decreases. The percentage change in the value of stiffness coefficients for direct fluid-film stiffness coefficient $\bar{S}_{xx}$ due to wear between L/D ratio of 0.5, 1.0 and 1.5 found to be more at higher L/D ratio of 1.5 when $\bar{\delta}_w > 0.2$ as reported in Table 3.

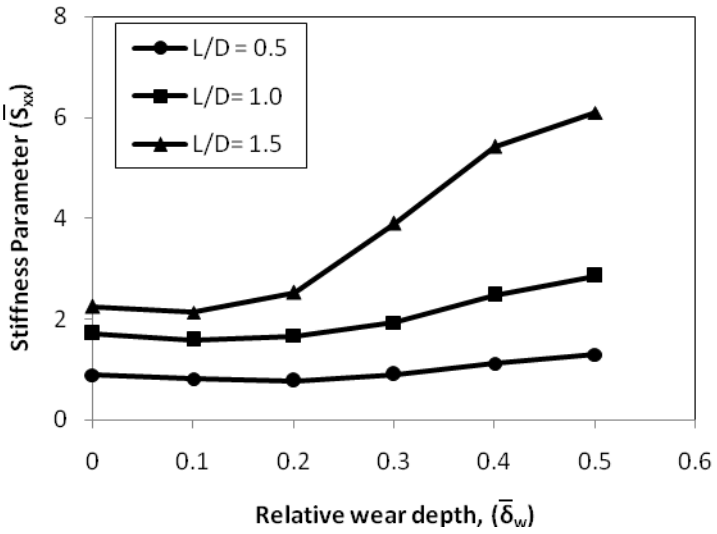

Figure 10: Direct fluid-film stiffness coefficient versus relative wear depth

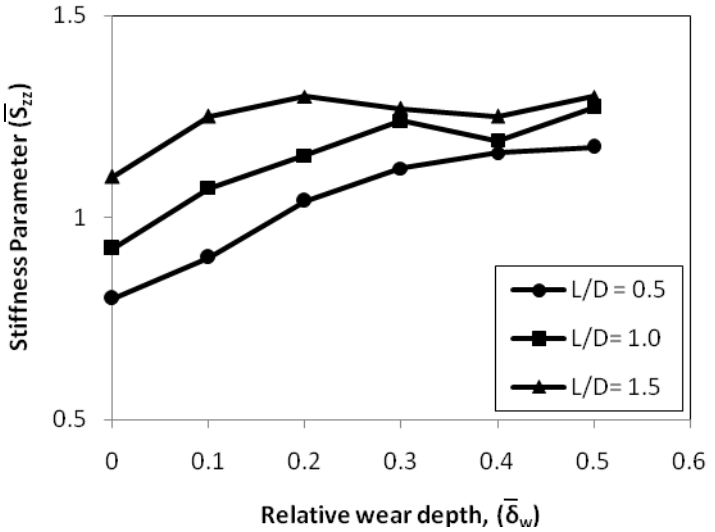

Figure 11: Direct fluid-film stiffness coefficient versus relative wear depth

The direct dimensionless damping coefficient parameters $\overline{C}_{xx}$ and $\overline{C}_{zz}$ as shown in fig.12 and Fig.13 shows a decreasing trend with an increase in L/D ratio. The percentage change in the value of damping coefficients for damping coefficient parameters $\overline{C}_{xx}$ and $\overline{C}_{zz}$ due to wear between L/D ratio of 0.5, 1.0 and 1.5 found to be more at higher L/D ratio of 1.5 and very low percentage variation in the value of

damping coefficient parameters ($\overline{C}_{xx}$ and $\overline{C}_{zz}$) was found for lower L/D ratio of 0.5 and 1.0 for all wear depth as reported in Table 3.

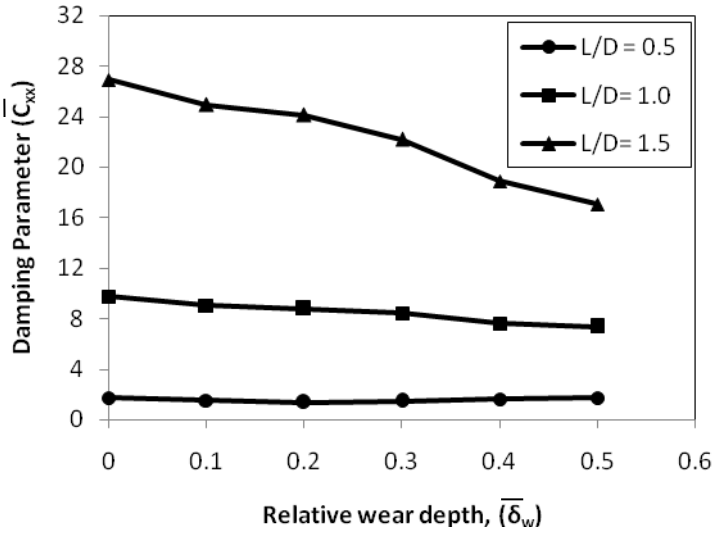

Figure 12: Direct fluid-film damping coefficient versus relative wear depth

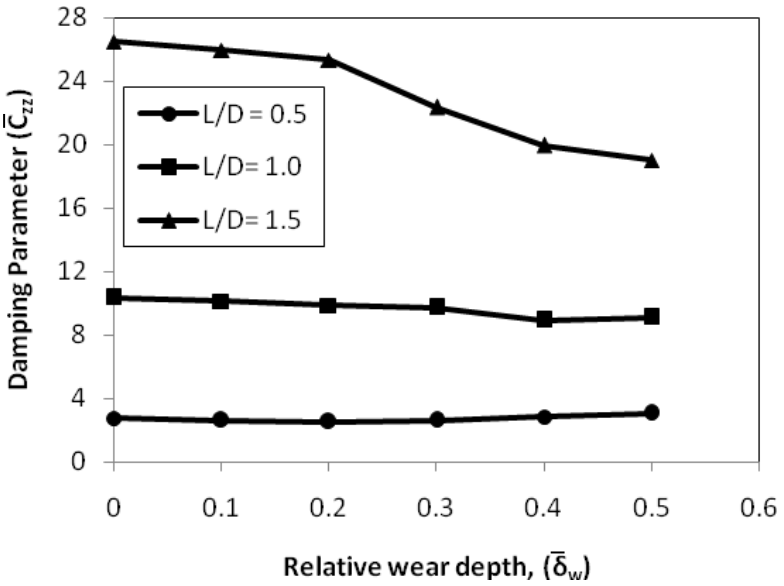

Figure 13: Direct fluid-film damping coefficient versus relative wear depth

In Fig.14 it is observed that the whirl ratio remains constant at higher L/D ratios and decreasing exponentially with the increase in relative wear depth. It can be seen that the whirling frequency ratio decreases more rapidly in lower L/D ratio equals to 0.5, which indicates better stability from the view point of whirl motion. The percentage change in the value of whirl ratio due to wear between L/D ratio of 0.5, 1.0 and 1.5 has been reported in Table 3 and found to be more at lower L/D ratio of 0.5.

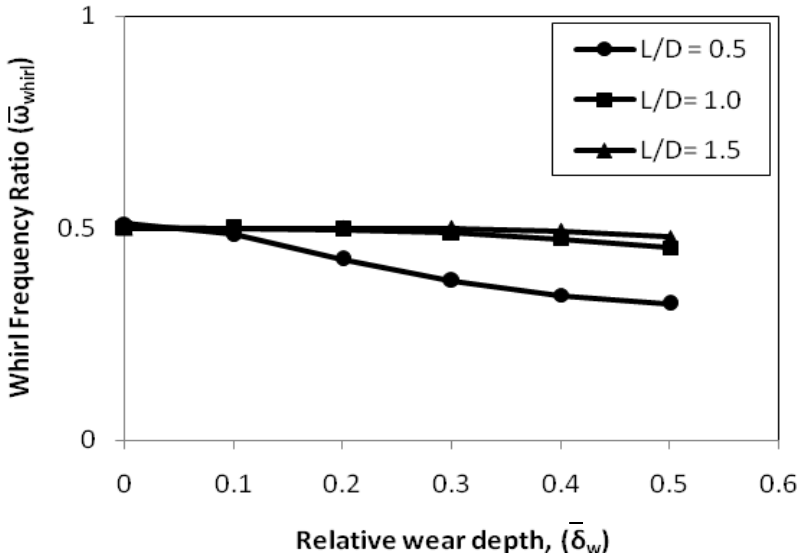

Figure 14. Whirl ratio versus relative wear depth

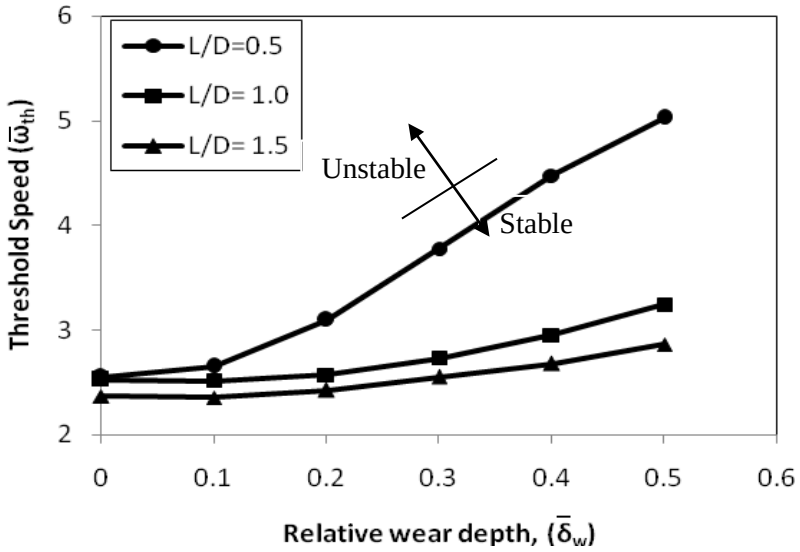

Figure 15. Threshold speed versus relative wear depth

The value of stability threshold speed decreases with an increase in L/D ratio and stability threshold speed margin increases as the wear depth parameter increases as shown in Fig .15. The lower and upper sides of each curve correspond to stable and unstable regions respectively. It is observed that the stability of worn journal bearings deteriorates with an increase in L/D ratio. This is due to the variation in the value of pressure gradients changes, and hence the value of bearing dynamic coefficient gets altered. Thus, the bearing stability threshold speed margin is expected to change. It is also observed that stability decrease first with an increase in wear depth and an improvement in stability is found after $\bar{\delta}_w > 0.2$ .The percentage change in the value of threshold speed due to wear between L/D ratio of 0.5, 1.0 and1.5 found to be more at lower L/D ratio of 0.5.

The simulated results of worn journal bearing with respect to relative wear depth for varying L/D ratio is presented. The percentage change in static and dynamic performance of hydrodynamic journal bearing operating under transient wear is reported in Table 2 and Table 3 respectively.

Table 2: Percentage change in static performance of hydrodynamic journal bearing operating under wear.

$\bar{\delta}_w$	L/D	$\%\varepsilon$	$\%\ \bar{p}_{\max}$	$\%\ \bar{h}_{\min}$	$\%\phi$	%f
0.1	0.5	1.75	25.2723	-1.167	-9.852	0.3003
0.2		8.25	43.7908	-5.5	28.188	1.5361
0.3		23.75	162.0915	-12.5	-48.617	5.1221
0.4		47.75	174.2919	-17.333	-63.8	13.0912
0.5		76.25	183.0065	-19.667	-72.311	28.5558
0.1	1.0	3.0864	22.2222	-0.597	-13.789	0.0188
0.2		17.284	48.9418	-3.341	-32.32	0.5001
0.3		46.2963	171.9577	-8.592	-50.11	1.5378
0.4		87.6543	191.0053	-13.723	-62.977	0.35319
0.5		140.7407	204.7619	-17.661	-71.866	7.1263
0.1	1.5	4.3478	23.2044	-0.441	-18.023	0.0442
0.2		28.2609	52.4862	-2.863	-41.205	0.2845
0.3		71.7391	179.0055	-6.828	-58.291	0.847
0.4		128.2609	201.6575	-10.352	-68.943	1.8584
0.5		202.1739	219.8895	-13.546	-75.827	3.6726

Table 3: Percentage change in dynamic performance of hydrodynamic journal bearing operating under wear

$\bar{\delta}_w$	L/D	$\%\,\bar{S}_{xx}$	$\%\,\bar{S}_{zz}$	$\%\,\bar{C}_{xx}$	$\%\,\bar{C}_{zz}$	$\%\,\bar{\omega}_{whirl}$	$\%\,\bar{\omega}_{th}$
0.1	0.5	-9.338	12.6271	-11.566	-4.44	-5.03	39.704
0.2		-13.672	30.1902	-20.843	-8.479	-16.53	21.4222
0.3		101.0213	40.2936	-16.231	-4.274	-26.43	47.9619
0.4		24.7775	45.0233	-6.25	4.3815	-33.17	75.4849
0.5		45.4427	46.8392	0.2301	11.0783	-37.05	97.0133
0.1	1.0	-6.963	16.303	-7.17	-2.29	-0.27	-0.485
0.2		-2.298	24.9837	-9.94	-4.84	-0.84	1.7688
0.3		112.9665	34.2084	-13.73	-6.01	-2.44	8.072
0.4		45.2624	29.0175	-21.72	-13.70	-5.15	16.6511
0.5		67.3125	37.8955	-24.41	-12.13	-9.51	28.2879
0.1	1.5	-5.152	13.462	-7.47	-1.92	00.0861188	-0.347
0.2		12.3452	18.0005	-10.41	-4.32	0.1341852	2.5087
0.3		173.2432	15.2774	-17.60	-15.58	600.829E-	7.9176
0.4		141.2756	13.462	-29.82	-24.72	05	13.2259
0.5		171.1333	18.0005	-36.71	-28.24	-1.177625	
						-4.093649	21.0509

4. CONCLUSION

This study investigates the effect of aspect ratio with varying wear depth on the performance of worn hydrodynamic journal bearings under transient conditions. Based on results, following conclusions can be drawn:

1) The effect of wear on all static and dynamic parameters is greater at lower L/D ratios.
2) The eccentricity ratio, maximum pressure, coefficient of friction, direct fluid-film stiffness coefficient and threshold speed increase with an increase in wear depth. The minimum fluid- film thickness, attitude angle, direct fluid-film damping coefficient and whirl frequency ratio decrease with an increase in wear depth.
3) The effects of relative wear depth due to wear in the stability threshold speed margin increases as the wear depth parameter increases. The whirling frequency ratio decreases more rapidly in lower L/D ratio equals to 0.5, which indicates better stability.
4) The stability of hydrodynamic journal bearings becomes progressively worse at higher L/D ratio. It decreases first with an increase in wear depth and an improvement in stability is found when $\bar{\delta}_w > 0.2$.

NOMENCLATURE

Dimensional Parameters

c : Radial clearance, mm

C_{ij} : Fluid-film damping coefficients ($i, j = x, z$), N.mm^{-2}

D : Journal diameter, mm

e : Journal eccentricity, mm

F : Fluid-film reaction ($\partial h/\partial t \neq 0$), N

F_x, F_z : Fluid-film reaction components in X and Y direction ($\partial h/\partial t \neq 0$), N

h : Nominal fluid-film thickness, mm

L : Bearing length, mm

M_c, M_J : Critical mass and Mass of journal, Kg

N : Rotational speed, rpm

O_B : Center of the bearing

O_j : Center of the journal

p : Pressure, N.mm^{-2}

p_s : Reference pressure, N.mm^{-2} ($\mu_r \omega_J R_J{}^2 / c^2$)

R_j, R_b : Radius of journal and bearing, mm

S : Sommerfeld Number

S_{ij} : Fluid-film stiffness coefficients ($i, j = X, Z$), N.mm^{-1}

t : Time, sec

W : Load Capacity, N

W_o : External load, N

x : Circumferential coordinate

y : Axial coordinate

X_J, Z_J : Journal center coordinate

X, Y, Z : Cartesian coordinate system

z : Coordinate along film thickness

Greek Letters

μ : Lubricant viscosity, Pa. sec

α : Angular coordinate, rad

ω_{rad} : Angular speed, rad.sec^{-1}

ϕ : Attitude angle, rad

δ_w : wear depth, mm

ω_{th} : Threshold speed, rad.sec^{-1}

ω_{whirl} : Whirl frequency, rad-sec^{-1}

Non-Dimensional Parameters

$\overline{C}_{ij} = C_{ij}\left(\dfrac{c^3}{\mu_r R_J^4}\right)$

$\overline{F}_x, \overline{F}_z = (F_x, F_z / p_s R_j^2)$

$\overline{h}, \overline{h}_{\min} = h/c,\ h_{\min}/c$

$\overline{p} = (p/p_s)$

$\overline{p}_{\max} = p_{\max}/p_s$

$\overline{S}_{ij} = S_{ij}\left(\dfrac{c}{p_s R_J^2}\right)$

$\bar{\tau} = t\left(c^2 p_s / \mu_r R_J{}^2\right)$

$\overline{W}_o = \dfrac{W_o}{p_s R_J^2}$

$(\overline{X}_J, \overline{Z}_J) = (X_J, Z_J)/c$

$(\overline{X}, \overline{Z}) = (X, Z)/c$

$\alpha, \beta = (x, y)/R_J$

$\varepsilon = e/c$

L/D = Aspect ratio

$\overline{\delta}_w = \delta_w / c$, worn depth

$\overline{\omega}_{th}$ $= \omega_{th}/\omega_J$

$\overline{\omega}_{whirl}$ $= \omega_{whirl}/\omega_J$

Ω $= \omega_J\left(\mu_r R_J^2/c^2 p_s\right)$, Speed parameter

Matrices

$\left[\overline{F}\right]$ = Assembled Fluidity Matrix,

$\{\overline{p}\}$ = Nodal pressure Vector,

$\{\overline{Q}\}$ = Nodal Flow Vector,

$\{\overline{R}_H\}$ = Column Vectors due to hydrodynamic terms,

$\{\overline{R}_{X_J}\}, \{\overline{R}_{Z_J}\}$ =Global right hand side vectors due to journal center linear velocities.

Subscripts and Superscript

b : Bearing

J : Journal

r : Reference value

max : Maximum value

min : Minimum value

. : First derivative w.r.t. time

REFERENCES

[1] Duckworth WE. and Forrestor PB. Wear of lubricated journal bearing, Proc.Inst. mech. Eng. Conf. on Lubrication and wear, London, Oct. 1957,714-719.

[2] Forrestor PB. Bearing and journal wear, Symposium. On wear in the gasoline Engine, Thomson Research Centre, Oct.1969, 75-91.

[3] Katzenmeier. G. The influence of materials and surface quality on wear behavior and load capacity of journal bearings, proc.Inst.Mech.Eng., Tribology Convention, 1972,Paper C/100/72,80-84.

[4] Mokhtar M.O., Howarth R.B. and Davies P.B, Wear characteristics of plain hydrodynamic journal bearings during repeated starting and stopping, ASLE Trans, 1978;20(3),191-194.

[5] Dufrane KF, Kannel JW and McCloskey TH. Wear of steam turbine journal bearings at low operating speeds. ASME J Lubricat Technol 1983; 105:313–17.

[6] Hashimoto H, Wada S and Nojima K. Performance characteristics of worn journal bearings in both laminar and turbulent regime. Part 1: Steady state characteristics. ASLE Trans 1986;29:565–71.

[7] Hashimoto H, Wada S and Nojima K. Performance characteristics of worn journal bearings in both laminar and turbulent regime. Part 2: Dynamic characteristics. ASLE Trans 1986;29.

[8] Vaidyanathan K and Keith TG. Performance characteristics of cavitated noncircular journal bearings in the turbulent flow regime. Tribol Trans 1991;34:35–44.

[9] Suzuki K and Tanaka M. Stability characteristics of worn journal bearings. In: Proceedings of the Asia-Pacific vibration conference, Kula Lumpur, 1995. p. 296–301.

[10] Kumar A and Mishra SS. Stability of rigid rotor in turbulent hydrodynamic worn journal bearings. Wear 1996;193:25–30.

[11] Kumar A and Mishra SS. Steady state analysis of non-circular worn journal bearings in non-laminar lubrication regimes. Tribol Int 1996;29:493–8.

[12] Fillon M, Bouyer J. Thermo hydrodynamic analysis of a worn plain journal bearing. Tribol Int 2004;37:129–36.

[13] Awasthi R.K, Sharma S.C and Jain S.C. Finite element analysis of orifice-compensated multiple hole-entry worn hybrid journal bearing, Finite Elements in Analysis and Design (2006;42: 1291 – 1303.

[14] Awasthi R.K, Sharma S.C and Jain S.C. Performance of worn non-recessed hole-entry hybrid journal bearings, Tribology International 2007; 40: 717–734.

[15]. Phalle Vikas M, Sharma S.C and Jain S.C. Performance analysis of a 2-lobe worn multirecess hybrid journal bearing system using different flow control devices Tribology International 52 (2012) 101–116.

[16] Kushare Prashant B and Sharma S.C. Nonlinear transient stability study of two lobe symmetric hole entry worn hybrid journal bearing operating with non-Newtonian lubricant TribologyInternational69(2014)84–101.

[17] Awasthi RK, The influence of wear and running-in on fluid-film journal bearing system -Thesis, Department of mechanical and industrial engineering ,Indian institute of technology roorkee, India 2006.

[18] Sharma RS, Chand S and Jain SJ, Performance Characteristics of Externally Pressurized Orifice Compensated Flexible Journal Bearing, STLE Tribology Transaction 1991;34:465-471.

[19] Sharma SC, Kumar V, Jain SC, Sinhasan R and Subramanian M, A Study of Slot-Entry Hydrostatic/Hybrid Journal Bearing using the Finite Element Method, Tribology International 1999;32:185-196**.**

[20] Sharma SC, Jain SC and Reddy NMM, A study of Non-recessed Hybrid Flexible Journal Bearing with Different Restrictors, STLE Tribology Transaction 2001;44(2):310-317.

[21] Chandrawat HN and Sinhasan R, A Study of Steady State and Transient Performance Characteristics of Flexible Shell Journal Bearing, Tribology International 1988;21:137-148.

[22] Smith DM, Journal Bearing in Turbo machinery, Chapman and Hall Ltd 1969.

[23] Nair V.P.S and Nair K.P, Finite element analysis of elastohydrodynamic circular journal bearing with micropolar lubricants, J. Finite Elem. Anal.Des.2004; 41; 75–89.

[24] Sharma SC, Phalle VM, Jain SC. Performance of a non circular 2-lobe multirecess hydrostatic journal bearing with wear. Ind LubrTribol 2012;64 (3):171–81.

[25] Kushare P and Sharma SC. A Study of two lobe non recessed worn journal bearing operating with non-Newtonian lubricant. Proc. I Mech Engg Part J: J Eng Tribol 2013;227(12):1418–37.